# Seeding with a harmonic optical klystron resonator configuration in a high repetition rate free electron laser

Hao Sun, Chao Feng,[*] Bart Faatz,[†] and Bo Liu[‡]

*Shanghai Institute of Applied Physics, Chinese Academy of Sciences, Shanghai 201800, China; University of Chinese Academy of Sciences, Beijing 100049, China and Shanghai Advanced Research Institute, Chinese Academy of Science, Shanghai 201210, China*

Georgia Paraskaki

*Deutsches Elektronen-Synchrotron DESY, 22607 Hamburg, Germany*

(Received 11 January 2022; accepted 26 May 2022; published 22 June 2022)

The generation of highly coherent radiation in a high repetition rate free electron laser driven by a superconducting linear accelerator has become a topic of growing interest. External seeding schemes like high-gain harmonic generation (HGHG) and echo-enabled harmonic generation are proven to be able to generate coherent radiation in the extreme ultraviolet and x-ray range. However, the repetition rate of current laser systems with sufficient power to modulate the electron beam is limited to the kilohertz range. Recently, to achieve seeding at a high repetition rate, an optical resonator scheme has been introduced to recirculate the radiation in the modulator to seed the electron bunches. In this paper, two harmonic optical klystron resonator configurations either starting with a seed laser or starting from shot noise are studied. With the harmonic optical klystron as the seeding source, the efficiency of harmonic radiation generation at a comparatively high harmonic can be significantly enhanced when compared with a standard single-stage HGHG. Simulation results show that highly coherent, stable, and high repetition rate pulses in the water window range could be generated by the proposed seeding schemes. Some practical considerations including beam energy chirp effects and the power density effects on mirrors are discussed.

DOI: 10.1103/PhysRevAccelBeams.25.060701

## I. INTRODUCTION

In most high gain free electron lasers (FELs) [1–3], the basic operational mode is self-amplified spontaneous emission (SASE) [4–6], which is initiated by the stochastic noise in the electron bunch. Therefore, SASE suffers from poor longitudinal coherence and large shot-to-shot fluctuations. To overcome these limitations, some seeding techniques like self-seeding [7,8] and external seeding [9–21] have been proposed. Self-seeding schemes can be used to improve temporal coherence, but they still suffer from large shot-to-shot energy fluctuations. External seeding schemes like high-gain harmonic generation (HGHG) [9–13] and echo-enabled harmonic generation (EEHG) [14–21] are triggered by stable, coherent external lasers, and, thus, their output radiation can be stable and coherent. However, the repetition rate of current laser systems with sufficient power to modulate the electron beam is limited to the kilohertz range.

To relax the power requirements of external seeding lasers in high repetition rate FELs, some methods, such as angular dispersion enabled microbunching (ADM) [22,23], self-amplification of coherent energy modulation (optical klystron) [24,25], and direct amplification enabled harmonic generation (DEHG) [26] were proposed. ADM can be used to relax the laser power requirement by using multidimensional manipulation of the electron beam. The optical klystron configuration is utilized to enhance the modulation at a fundamental wavelength to decrease the required seed laser power which has been experimentally confirmed at the Shanghai soft x-ray FEL test facility [24,27]. DEHG uses a relatively long modulator as the media for laser amplification and energy modulation to relax the requirement of laser power.

Cavity-based FELs including the x-ray FEL oscillator (XFELO) [28–30] and regenerative amplifier free electron lasers [31–33] have been proposed as a direct source of coherent x rays at high repetition rate. Furthermore, the XFELO or extreme ultraviolet FEL oscillators can also be used as a source of seed for subsequent cascades [34–36]. Recently, for seeding at a high repetition rate, another

[*]fengchao@zjlab.org.cn
[†]faatzbart@sari.ac.cn
[‡]liubo@zjlab.org.cn

optical cavity-based FEL scheme has been introduced to recirculate the radiation in the modulator to seed the high repetition rate electron bunches. Earlier studies [37–39] show that an in-cavity modulator combined with an amplifier in an HGHG configuration can be used to generate radiation whose wavelength can reach the water window region. This scheme overcomes the limitation of requiring high repetition rate seed laser systems. This is important for future continuous wave machines such as SHINE [40] and LCLS-II [41], and it is also an alternative for burst-mode machines like FLASH [42,43] and European XFEL [44]. For the optical resonator scheme, this can be done either with a seed laser at a low repetition rate to initiate the process, or it can start from shot noise, where the main challenge is to get the system to saturate at a low power to avoid inducing a large energy spread in the electron beam, which limits the FEL performance at short wavelength in a standard single-stage HGHG [9]. At the same time, the intensity of the amplified light field in the resonator is quite intense, and the heat load of the mirrors is significant.

The harmonic optical klystron concept is studied in Ref. [45] to enhance self-amplified spontaneous emission or introduced as a harmonic cascade method in Ref. [46]. In this paper, a harmonic optical klystron resonator configuration is proposed for seeding a high repetition rate free electron laser. Similar to Ref. [46], instead of using a single modulator, the modulator is divided into two parts separated by a chicane as shown in Fig. 1 (middle and bottom). The first part of the harmonic optical klystron resonator is used for providing the seed which is initiated by a low repetition rate laser or starts from shot noise, and the second part is tuned to a harmonic of the first modulator. As long as the laser power in the first part is constant, the bunching factors at fundamental and harmonics are constant. The proposed scheme has three advantages: First, it can generate seeded FEL radiation at a high repetition rate, overcoming the repetition rate limitation of current laser systems. In addition, with the harmonic optical klystron scheme as the seeding technique, the efficiency of harmonic radiation generation is increased, and higher harmonics than in a standard single-stage HGHG can be achieved. Furthermore, the required energy modulation in the first modulator of the harmonic optical klystron resonator is not large, so the intensity of the amplified light field in the resonator is further reduced that can relieve the thermal load on the mirrors.

The remaining part of this paper is organized as follows. The harmonic optical klystron resonator-radiator configuration is introduced and discussed in Sec. II. We study the harmonic optical klystron resonator radiator in detail for a single pass in Sec. III. The multipass simulation results of harmonic optical klystron resonator radiator, including starting from an external seed laser and starting from shot noise, is presented in Sec. IV. In addition, some practical considerations including beam energy chirp effects and the

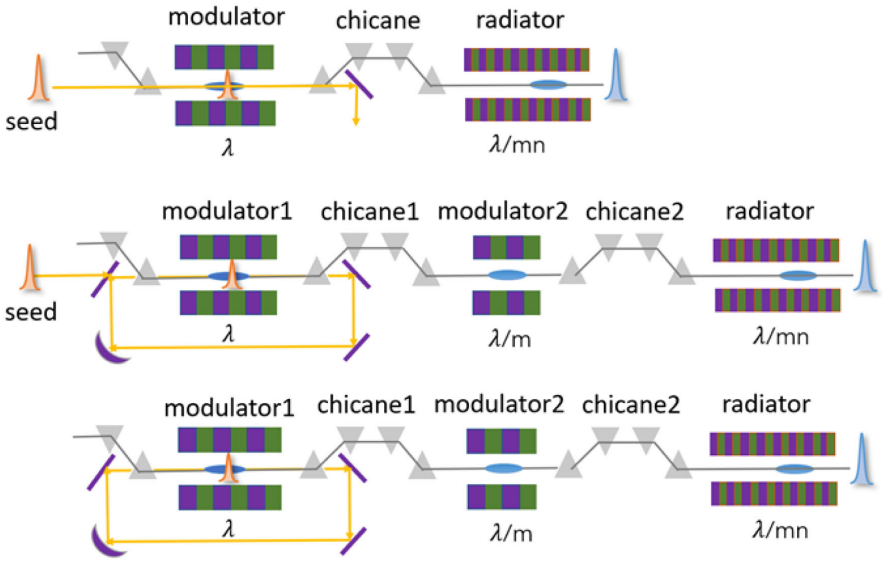


FIG. 1. In a standard single-stage HGHG scheme (top), the modulator is resonant at the fundamental wavelength of the seed laser, and chicane is responsible for density modulation; the radiator is tuned to a harmonic of the seed laser wavelength. In the harmonic optical klystron resonator-radiator configuration, either starting with an external seed laser (middle) or starting from shot noise (bottom), we need a pair of modulator-chicane modules. Modulator 1 is resonant at the fundamental wavelength of the seed laser, and modulator 2 is tuned to a harmonic of the first modulator. Chicane 1 is responsible for increasing the bunching at the fundamental wavelength, while chicane 2 is responsible for longitudinal density modulation at a harmonic of the seed laser wavelength. The final FEL amplification of high harmonic radiation is taking place in the radiator.

power density effects on mirrors are discussed in Sec. V. Finally, we summarize this work and give a outlook in Sec. VI.

## II. HARMONIC OPTICAL KLYSTRON RESONATOR-RADIATOR CONFIGURATION

Layouts for the proposed technique, namely, harmonic optical klystron resonator radiator are shown in Fig. 1. In this setup (Fig. 1, middle and bottom), the modulator is divided into two parts separated by a chicane, and the first modulator is resonant at the fundamental wavelength of the seed laser. The second modulator is tuned to a harmonic of the first modulator. In the first modulator, a small energy modulation of the electron beam is induced, and it is transformed into a density modulation after traversing through the first chicane with a longitudinal dispersion $R_{56,1}$. Then, the electron beam is modulated at the harmonic of the seed laser wavelength in the second modulator. A density modulation occurs at a harmonic of the seed laser wavelength when the electron beam traverses through the second chicane. Finally, the FEL amplification of a harmonic of the seed laser wavelength is taking place in the radiator. In this paper, we consider two approaches to generate and store a seed laser pulse in the harmonic optical klystron resonator, as shown in Fig. 1. In the first case (Fig. 1, middle), a low repetition rate seed laser is injected into the resonator for the first pass. The power of the seed laser is amplified by its interaction with the electron bunch in the first modulator of the harmonic optical klystron resonator, and the optical field is stored in an optical cavity to seed the next electron bunch arriving at the first modulator. Therefore, the gain is needed only to compensate for cavity losses. In the second case (Fig. 1, bottom), the radiation is initially generated by the electron beam shot noise and amplified by the following electron bunches in the resonator. In the next simulations, we use the typical parameters of a soft x-ray FEL. The electron beam parameters are summarized in Table I. The simulations are performed by combining two codes: Genesis 1.3 [47] and Ocelot [48].

TABLE I. Parameters for simulation.

| Parameter | Value |
|---|---|
| Energy ($E$) | 2530 MeV |
| Current flattop | 800 A |
| Bunch length (FWHM) | 110 fs |
| Repetition rate | 1 MHz |
| Charge | 100 pC |
| Emittance | 0.5 mm · mrad |
| Uncorrelated energy spread ($\sigma_E$) | 164 keV |
| Laser wavelength ($\lambda$) | 50 nm |
| Modulator 1 length/period length/$K$ | 6 m/0.05 m/9.80 |
| Modulator 2 length/period length/$K$ | 3 m/0.05 m/4.75 |
| Radiator length/period length/$K$ | 15 m/0.02 m/3.21 |

## III. HARMONIC OPTICAL KLYSTRON RESONATOR RADIATOR FOR A SINGLE PASS (WITH SEED LASER)

### A. Harmonic optical klystron HGHG (HOK HGHG) scheme

To generate coherent radiation in the water window range, here we tune the second modulator to the fourth harmonic ($m = 4$) of the seed laser, and the radiator is tuned to the fifth ($n = 5$) harmonic of this wavelength, which is the 20th harmonic of the seed laser wavelength as shown in Fig. 1. The simulation parameters of the first modulator and the first chicane for a resonator scheme can be optimized according to the procedure in Ref. [38]. In our case, the length of the first modulator in a resonator should be longer than the modulator used in a single pass to offer sufficient power gain to compensate for the cavity losses. For the first modulator in the HOK HGHG scheme, the normalized energy modulation amplitude is defined as [49]

$$A_1 = \frac{\Delta E_1}{\sigma_E}, \tag{1}$$

where $\sigma_E$ is the energy spread in the modulator exit and the energy modulation can be calculated by [49]

$$\Delta E_1 = \sqrt{\frac{P_{\mathrm{mod}}}{P_o}}\frac{m_e 2KL_u \mathrm{JJ}}{\gamma w_0}, \tag{2}$$

where $w_0$ is the seed laser transverse waist size, $L_u$ is the modulator length, $K$ is the dimensionless undulator parameter, $m_e$ is the electron mass, $P_o$ is a constant value about 8.7 GW, $\mathrm{JJ} = J_0(\xi) - J_1(\xi)$, $\xi = K^2/(4 + 2K^2)$, and $J_{0,1}$ is the Bessel function of the zeroth and first order. For a long modulator, $P_{\mathrm{mod}}$ is the laser power after two-thirds of the modulator length [38,50]. For the first chicane, the normalized dispersion is defined as [49]

$$B_1 = \frac{2\pi R_{56,1}\sigma_E}{\lambda E}, \tag{3}$$

where $\lambda$ is the seed laser wavelength and $E$ is the electron beam energy. The bunching factor at the $m$th harmonic of the seed laser after the first chicane can be represented as [49]

$$b_m = J_m(-mA_1B_1)\exp\left(-\frac{1}{2}m^2B_1^2\right), \tag{4}$$

where $J_m$ is the Bessel function of the first kind.

In our simulation, the input seed laser power at 50 nm is set to $P_{\mathrm{mod}} = 1.7$ MW, and the length of the first modulator is set to 6 m to offer sufficient power gain to compensate the cavity losses. The input seed power profile is shown by a solid black line in Fig. 2, and the power can be amplified to about 13.8 MW after the first modulator,

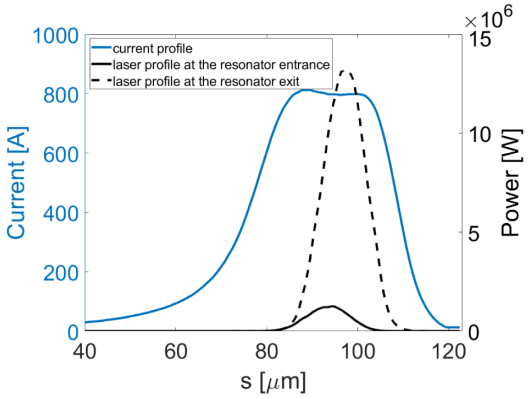


FIG. 2. The beam current distribution (blue line) and seed laser power profile for the single pass (solid black line, at the entrance of the first modulator; dotted black line, at the exit of the first modulator).

which is represented by a dotted black line in Fig. 2. The normalized energy modulation amplitude $A_1 = 4.8$, and the normalized dispersion needs to be optimized by Eq. (4). The $R_{56,1}$ is set to 30 $\mu$m to make sure there is sufficient bunching at the entrance of the second modulator. The longitudinal phase space of electron beam at the exit of the first dispersion section is shown in Fig. 3(a). In the second modulator, the prebunched beam can be modulated at the harmonic of the seed laser wavelength in addition to emitting coherent harmonic radiation. The radiation power grows quadratically when the length of the modulator is short and exponentially when the length is long. To preserve the quality of the electron beam as much as possible, the length of the second modulator needs to be optimized. The harmonic energy modulation amplitude can be simplified as [50]

$$A_2 = \frac{Eb_m}{3\sigma_{E_1}}\rho_2 L_2^2, \tag{5}$$

where $b_m$ is the $m$th harmonic bunching factor of the electron beam at the entrance of the second modulator, $\rho_2$ is the Pierce parameter in the second modulator, $L_2$ is the ratio of the second modulator length to the gain length, and $\sigma_{E_1}$ is the energy spread after the first modulator.

In our case, $L_2 = 3$, $\sigma_{E_1} = 552$ keV, $b_m \approx 0.17$, $E = 2530$ MeV, and $\rho_2 \approx 0.002$, resulting in $A_2 \approx 4.6$. When the electron beam passes through the second chicane, the bunching factor at the $m \times n$th harmonic of the seed laser can be calculated as [50]

$$b_{m\times n} = J_n(-nA_2B_2)\exp\left(-\frac{1}{2}n^2B_2^2\right), \tag{6}$$

where $J_n$ is the Bessel function of the first kind. For the second chicane, the normalized dispersion is defined as [50]

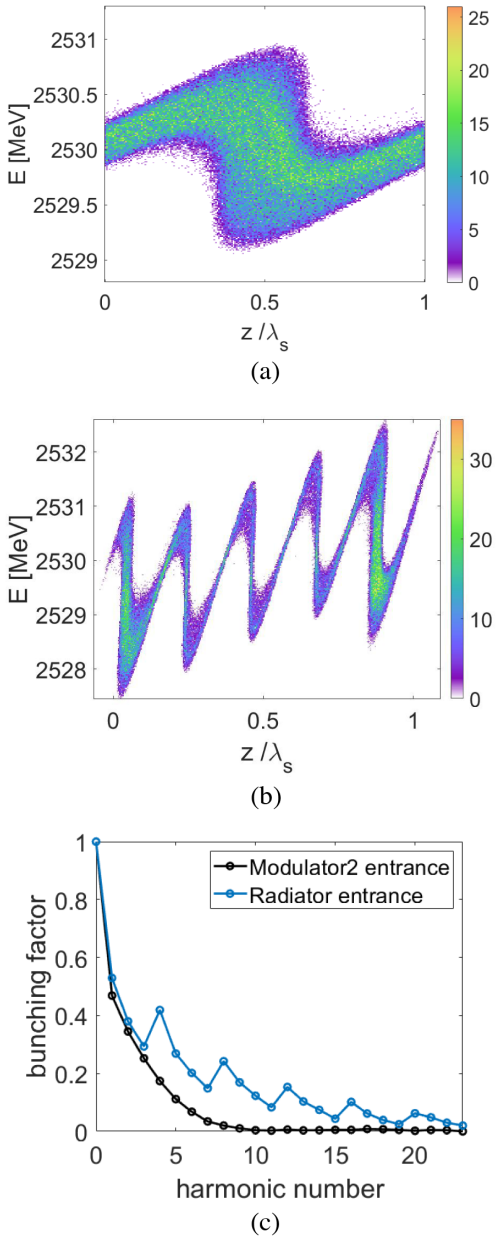


FIG. 3. (a) Longitudinal phase space of the electron bunch at the entrance of modulator 2 and (b) at the entrance of the radiator. (c) Bunching factor for different harmonics at the entrance of modulator 2 and at the entrance of the radiator ($R_{56,1} = 30$ $\mu$m, $R_{56,2} = 4$ $\mu$m).

$$B_2 = \frac{2\pi R_{56,2}\sigma_{E_1}}{\lambda_m E}, \tag{7}$$

where $\lambda_m = \lambda/m$. For the case $A_2 \approx 4.6$, the value of $R_{56,2}$ of 4 $\mu$m is estimated by Eq. (7) and optimized in Genesis 1.3 simulation. When the electron beam passes through the second chicane, the longitudinal phase space of the electron bunch is shown in Fig. 3(b), and the bunching occurs at higher harmonics as represented by the blue line in Fig. 3(c).

It can be seen that the electron beam still has a bunching factor of 6.20% on the 20th harmonic of the seed laser.

In the first modulator of the HOK HGHG scheme, an energy modulation $A_1 = 4.8$ is induced and some additional energy spread is introduced accordingly. The energy spread after the first modulator of the HOK HGHG scheme is 552 keV in the simulation. Then, the electron beam passes through the second modulator with a length of 3 m, and the energy spread $\sigma_{E_2}$ increases to 916.8 keV due to the coherent emission generated in the second modulator. For the simulation parameters in Table I, the Pierce parameter $\rho_r$ in the radiator which is resonant at 2.5 nm is 0.001. In the proposed HOK HGHG scheme, $\sigma_{E_2}/E = 3.6 \times 10^{-4} \ll \rho_r$, which is beneficial to the FEL gain.

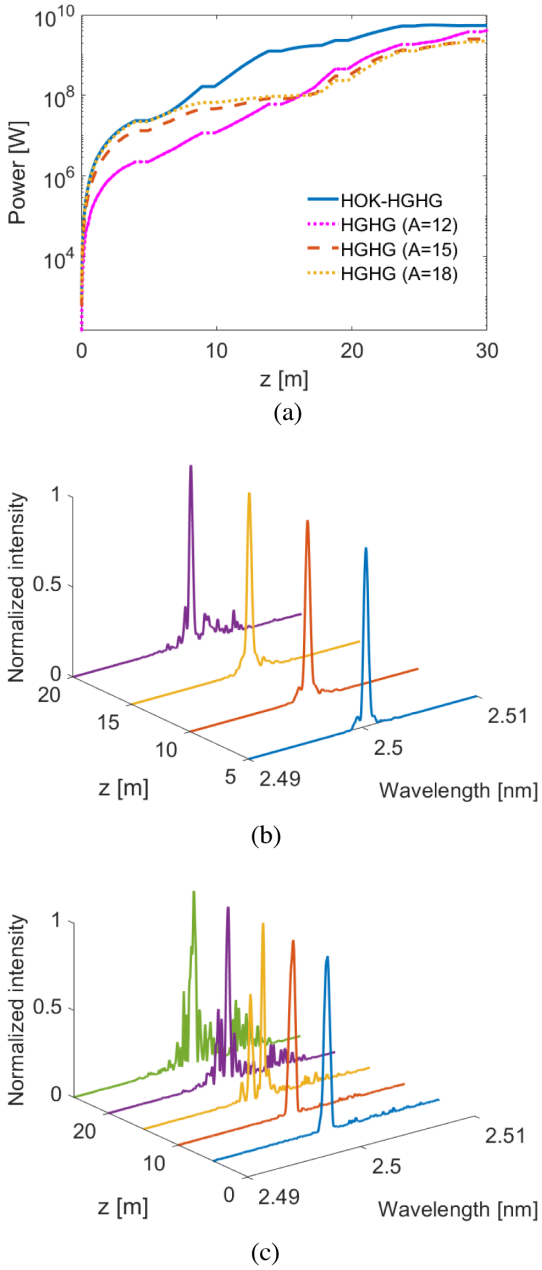


FIG. 4. (a) The gain curves for an FEL output wavelength of 2.5 nm along the radiator for the four cases [HOK HGHG and the standard single-stage HGHG ($A = 12$, 15, 18)]. The output spectrum profiles at different locations along the radiator for (b) the HOK HGHG scheme and (c) the standard single-stage HGHG ($A = 15$).

### B. Radiation performances

In this section, we present the radiation performances of the HOK HGHG scheme for a single pass. The electron beam with a bunching of 6.20% at the 20th harmonic of the seed laser is sent into a radiator for FEL amplification. The gain curve along the radiator is shown in Fig. 4(a). It can be seen that the peak power of the radiation grows exponentially and reaches saturation at 15 m with a gigawatt level. The output spectrum at saturation is shown by the yellow curve in Fig. 4(b), where the calculated FWHM bandwidth is $1.78 \times 10^{-4}$, which signifies the excellent temporal coherence of the radiation.

In addition, the proposed HOK HGHG scheme is compared with the standard single-stage HGHG scheme. For the standard single-stage HGHG scheme, in order to get bunching at the 20th harmonic, the required energy modulation amplitude is larger than 10 at least [51]. In the meantime, in order to achieve FEL exponential amplification, the energy spread of the electron beam at the entrance of the radiator has to fulfill the requirement of $\sigma_{E_r}/E \ll \rho_r$, where $\rho_r$ is the Pierce parameter [2,52]. For the simulation parameters in Table I, the Pierce parameter $\rho_r$ in the radiator which is resonant at 2.5 nm is 0.001; therefore, the requirement $\sigma_{E_r}/E \ll \rho_r$ leads to $\sigma_{E_r} = \sqrt{\sigma_E^2 + \Delta E^2/2} \ll 2.53$ MeV, which is equivalent to $A = \Delta E/\sigma_E \ll 22$. Therefore, we determine the value range of energy modulation amplitude.

We optimize three cases in standard single-stage HGHG mode with an energy modulation of 12, 15, and 18, respectively, to generate effective bunching at the 20th

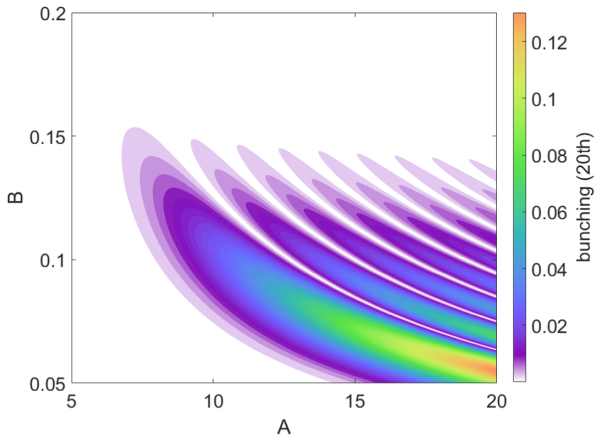


FIG. 5. The dependence of the bunching factor of the 20th harmonic with respect to the two parameters $A$ and $B$ ($A = \frac{\Delta E}{\sigma_E}$ and $B = \frac{2\pi R_{56}\sigma_E}{\lambda E}$) in a standard single-stage HGHG scheme.

TABLE II. Overview of output radiation simulations. The final FEL radiation is resonant at 2.5 nm, which is the 20th harmonic of the seed laser wavelength in the four cases. For the energy spread and bunching, the values are calculated from the entrance of the radiator.

| | Bunching at the 20th harmonic | Energy spread (rms) | Saturation length |
|---|---|---|---|
| HGHG ($A = 12$) | 3.00% | 1401 keV | 30 m |
| HGHG ($A = 15$) | 5.00% | 1747 keV | 27 m |
| HGHG ($A = 18$) | 8.00% | 2094 keV | 21 m |
| HOK HGHG | 6.20% | 917 keV | 15 m |

harmonic of the seed laser. The working points for the three cases are optimized based on Eq. (4). The dependence of the bunching factor of 20th harmonic respect to the two parameters $A$ (normalized energy modulation amplitude) and $B$ (normalized dispersion) is shown in Fig. 5. The gain curve along the radiator for the standard single-stage HGHG with energy modulations of 12, 15, and 18 are shown in Fig. 4(a), and some FEL parameters are summarized in Table II. It can be seen that the case with energy modulation of 12 has a small bunching of 3% and a long saturation length of 30 m. For the cases with energy modulation of 15 and 18, even though they have higher initial bunching of 5% and 8%, respectively, the FEL performances are poorer due to the induced larger energy modulation. Taking the standard single-stage HGHG with energy modulation of 15 as an example, the output spectrum profiles of FEL radiation at different locations along the radiator are shown in Fig. 4(c). As shown in this figure, the radiation pulse shows highly temporal coherence in the early part of the radiation section but deteriorates in longitudinal coherence from the 15-m mark to the saturation. Because of the long saturation length required, the SASE background becomes non-negligible as it becomes visible in Fig. 4(c). In conclusion, the HOK HGHG scheme is more advantageous in generating comparatively high harmonic radiation, such as a shorter saturation length and a higher signal-to-noise ratio of the radiation.

## IV. HARMONIC OPTICAL KLYSTRON RESONATOR RADIATOR FOR MULTIPASS

### A. Harmonic optical klystron resonator radiator starting with an external seed laser

In this section, we show multipass simulation results of the harmonic optical klystron resonator radiator, which starts with an external seed laser. In the simulation, we use the electron beam parameters summarized in Table I. The FEL process in the undulator is simulated with three-dimensional time-dependent code Genesis 1.3, and the optical field in the cavity is treated with Ocelot, which accounts for the slippage, reflectivity, and focusing. A fresh bunch is used to interact with an ideal Gaussian seed laser in the first modulator of the HOK resonator for the first pass. At the end of the first modulator, the optical field is saved, and the electron beam travels through the rest of the HOK resonator and the radiator. For the implementation of the cavity in the simulations, we consider a simplified cavity that allows faster simulations. The ring cavity is composed by four mirrors, two of which focus. Taking into account the losses of all mirrors, the total round-trip loss is 91%. The repetition rate of 1 MHz requires a cavity of 300 m round-trip length, while for the 4.5 MHz of the burst-mode machines this is reduced to 66 m. For optimum longitudinal overlap in each round-trip, we detune the cavity length to account for the slippage. In our case, we need to detune the cavity by 3.5 $\mu$m to achieve this. The manipulated field file is loaded into Genesis 1.3 for the next pass in the first modulator in which it interacts with a fresh bunch again. Finally, a different random seed for shot noise calculation is used to account for the effect of the bunch to bunch fluctuations.

In our simulation, we use a 50 nm laser with a low repetition rate of 10 Hz for the first pass, which is generated by high harmonic generation (HHG). Experiments confirm that the HHG can be utilized to achieve microjoules of pulse energy at low repetition rates down to a wavelength of 50 nm [53]. The input seed laser power at 50 nm is set to 20 MW, the total reflectivity of the cavity is set to 9%, and the length of the first modulator is set to 6 m to offer sufficient power gain to compensate for the cavity losses. The wavelength of the final radiation is 2.5 nm, which is the 20th harmonic of the 50 nm seed laser. In Fig. 6, we present

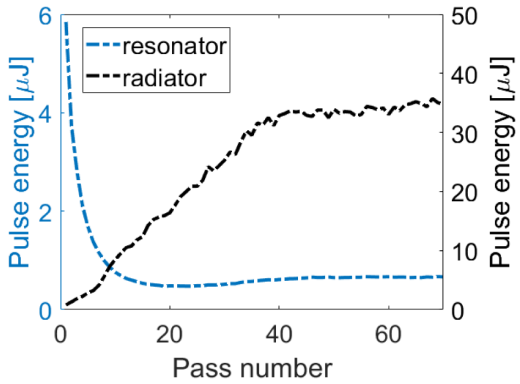


FIG. 6. Overview of the photon pulse energy per pass in the resonator (at the end of the modulator, left scale) and in the radiator (at the end of the radiator, right scale). The output wavelength of the simulation is 2.5 nm, which is the 20th harmonic of the 50 nm seed.

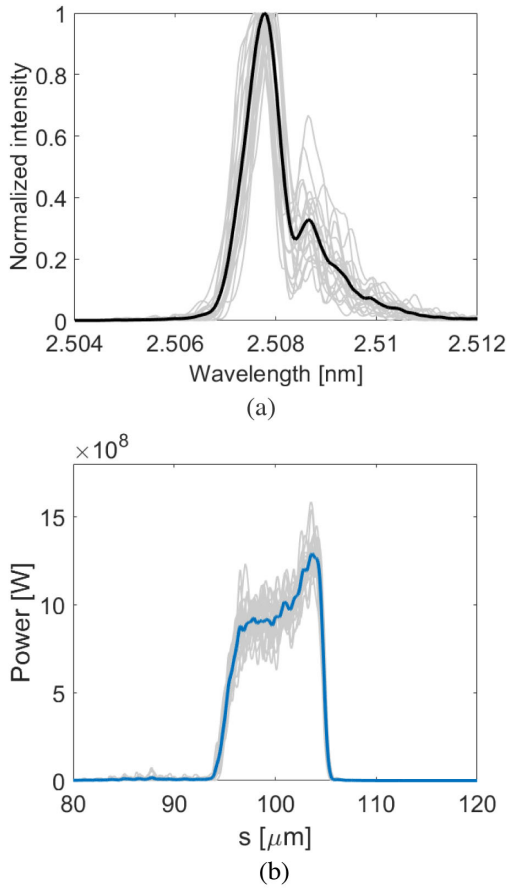


FIG. 7. (a) Output spectrum profiles at the end of the radiator (gray lines represent the 38th–70th passes, and the black line represents the average spectrum over the 38th–70th passes). (b) Output power profiles at the end of the radiator (gray lines represent the 38th–70th passes, and the blue line represents the average power over the 38th–70th passes).

the photon pulse energy per pass in the resonator and the radiator. The whole system is stabilized after around 38 passes with estimated root-mean-square (rms) fluctuations of pulse energy being 1.0% in the resonator and 2.3% in the radiator. After the whole system enters the steady-state region, the stabilities in the frequency domain and time domain for the final FEL radiation are shown in Fig. 7. The spectrum profiles from the 38th to the 70th pass are shown in Fig. 7(a), and the power profiles for the same passes are shown in Fig. 7(b). For the final FEL radiation, the spectrum and power profiles are stable after the system enters the steady-state region. In addition, the spectrum of the multipass FEL radiation is shifting toward longer wavelengths, which results from an induced time dependence of the phase of the FEL radiation [37]. For the multipass simulation, the average one in the steady-state regime is used to compare with the single-pass simulation in the time and frequency domain as shown in Table III. The pulse length of the multipass FEL radiation is shorter

TABLE III. Properties of 2.5 nm FEL output radiation. For the multipass HOK HGHG resonator-radiator simulations starting from an external seed laser, the pulse energy, the FWHM pulse duration, and the relative FWHM bandwidth are the average ones in the steady-state regime of the system.

| | Single-pass | Multipass |
|---|---|---|
| Output pulse energy | 45.1 $\mu$J | 34.2 $\mu$J |
| FWHM pulse duration | 46.2 fs | 37.3 fs |
| $\Delta\lambda_{\mathrm{FWHM}}/\lambda$ | $1.7 \times 10^{-4}$ | $3.1 \times 10^{-4}$ |

and the relative bandwidth is wider compared to the single-pass radiation, which is caused by the development of an FEL frequency chirp along the first modulator with the number of passes [37].

The pulse properties in the cavity, such as the pulse duration and bandwidth, can be controlled through altering the characteristics of the injected seed laser, on the one hand. On the other hand, previous studies show that the cavity length detuning can be used to control the pulse duration, bandwidth, and pulse energy of the radiation in the cavity [32,38,54]. In Fig. 8, we show the detuning curve with the pulse energy and FWHM pulse duration averaged over 40 passes in the cavity. In Fig. 8, $\Delta L_{\mathrm{cav}} > 0$ means that the cavity length is longer than the zero-detuning length, which is defined as the length of the cavity for which the light pulse overlaps with the following electron bunch without taking into account the slippage [38]. The pulse duration and pulse energy of the radiation in the cavity can be controlled via the cavity length detuning.

### B. Harmonic optical klystron resonator radiator starting from shot noise

Alternatively, one can also start from noise and not use a seed laser at all. In this case, the complete process can be divided into two phases, namely, the "buildup regime" and the "steady-state regime" [39]. The net gain per pass in the

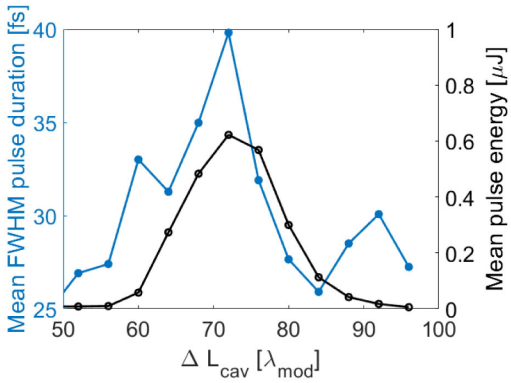


FIG. 8. Mean pulse duration (blue line) and pulse energy (black line) over 40 passes in the cavity for different cavity length detunings $\Delta L_{\mathrm{cav}}$. The modulator in the cavity is tuned to $\lambda_{\mathrm{mod}} = 50$ nm.

buildup regime needs to be positive to build up the peak power required for seeding. In the steady-state regime, the power downstream of the modulator in the cavity needs to be well below the "natural" saturation to avoid large induced energy spread, which would be beneficial to the amplification process at the radiator. Therefore, the net gain needs to go back zero to keep the balance between the power gain and the resonator power loss, and the intracavity power can be maintained at a low level for effective seeding. For a transition from positive gain to zero net gain, the gain has to be reduced. Several different methods to control the power gain are discussed in Ref. [39]. In this paper, we control the net gain by adjusting the attenuation of intracavity radiation as shown in Ref. [39]. In the buildup regime, the reflectivity is as high as estimated at 50 nm to build up the desired peak power. To reduce the net gain in the modulator, we reduce the total reflectivity in the resonator.

In this case, we use the same set of simulation parameters summarized in Table I, and the first modulator of the resonator is resonant at 50 nm wavelength. As shown in Fig. 9, 38 passes are required in the buildup regime to reach an energy modulation $A_1 = 4.8$ with $R_{\text{buildup}} = 7.8\%$. From the 38th pass and onward, the total reflectivity is reduced to 5.8% to keep the zero net gain. The whole system is stabilized with estimated rms fluctuations of pulse energy being 2.3% in the resonator and 4.0% in the radiator. After the whole system enters the steady-state region, the stabilities in the frequency domain and time domain for the final FEL radiation are shown in Fig. 10. The spectrum profiles from the 38th to the 70th pass are shown in Fig. 10(a), and the power profiles for the same passes are shown in Fig. 10(b). As is the case starting with an external seed laser, the spectrum of the multipass FEL radiation is shifting toward longer wavelengths, which results from an induced time dependence of the phase of the FEL radiation [37]. The multipass FEL simulation results are summarized in Table IV. Compared to the case starting from an external seed laser, the final FEL radiation pulse properties such as peak power, pulse duration, spectral bandwidth, and stability are roughly the same.

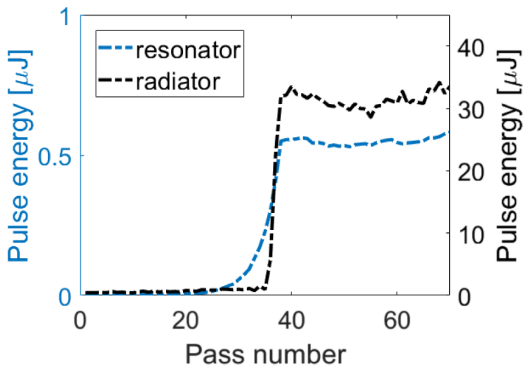


FIG. 9. Overview of the photon pulse energy per pass in the resonator (at the end of the modulator, left scale) and in the radiator (at the end of the radiator, right scale) for the case starting from shot noise.

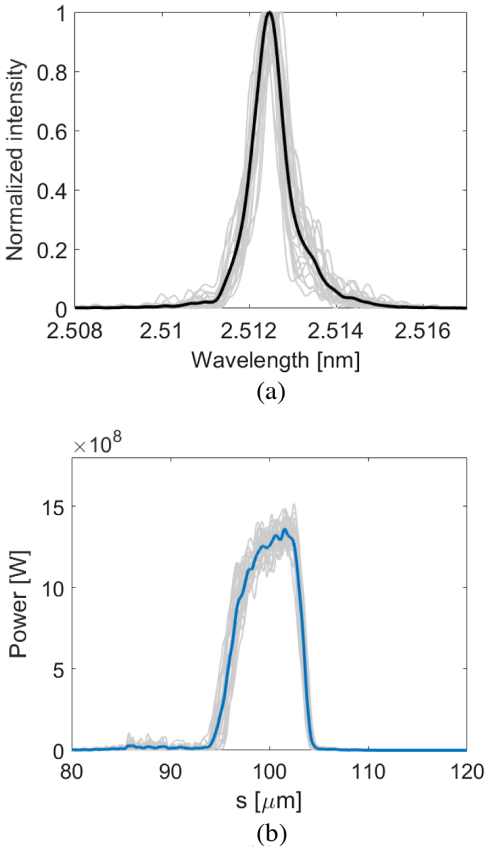


FIG. 10. (a) Output spectrum profiles at the end of the radiator (gray lines represent the 38th–70th passes, and the black line represents the average spectrum over the 38th–70th passes). (b) Output power profiles at the end of the radiator (gray lines represent the 38th–70th passes, and the blue line represents the average power over the 38th–70th passes).

### C. Transverse property of stored radiation in the cavity

In this section, we investigate the transverse property of the stored radiation in the cavity. In FEL physics, the transverse property of the radiation pulse plays an important role in the energy modulation process and

TABLE IV. Properties of 2.5 nm FEL output radiation. For the multipass HOK resonator-radiator simulations starting from shot noise, the pulse energy, the FWHM pulse duration, and the relative FWHM bandwidth are the average ones in the steady-state regime of the system.

| | Multipass |
|---|---|
| Output pulse energy | 31.2 $\mu$J |
| FWHM pulse duration | 30.6 fs |
| $\Delta\lambda_{\text{FWHM}}/\lambda$ | $2.6 \times 10^{-4}$ |

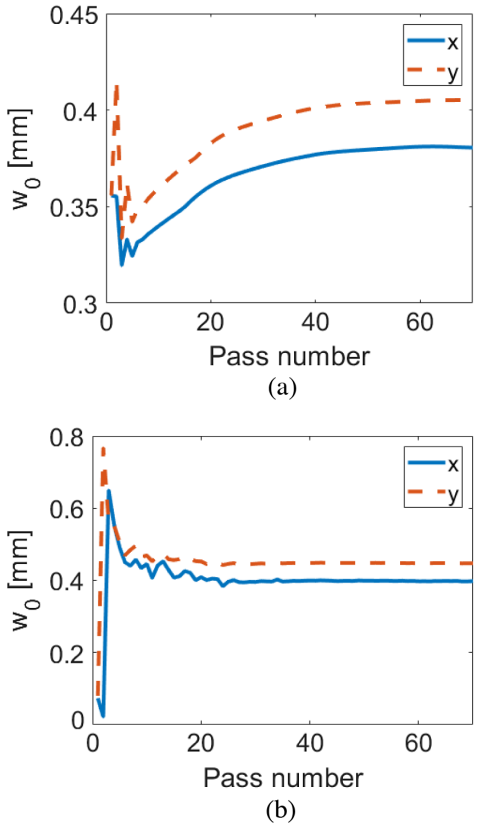


FIG. 11. The transverse size of a stored radiation pulse in the cavity per pass on the horizontal (x) and vertical (y) plane. (a) Case starting with an external seed laser. (b) Case starting from shot noise.

amplification process that occur in an undulator [49]. For the resonator, the transverse property of the stored radiation affects the gain process and stability of the system. The waist size of the stored radiation per pass on the horizontal (x) and vertical (y) planes is shown in Fig. 11 for both cases starting with an external seed laser and starting from shot noise. The waist size $w_0$ in Fig. 11 is defined as the radius of the beam when the intensity drops to $1/e^2$ of the on-axis intensity and at focus position when propagating in a drift section. In the case starting from an external seed laser, the seed laser is an ideal Gaussian pulse in the first pass, and the transverse size of the stored radiation stabilizes after the system enters the steady-state region, which is determined by gain guiding in the cavity as shown in Fig. 11(a). In the case starting from shot noise, the spontaneous radiation from shot noise is stored in the cavity, and its transverse size stabilizes after several tens of passes as shown in Fig. 11(b).

## V. PRACTICAL CONSIDERATIONS

### A. Beam energy chirp effect in the HOK HGHG scheme for a single pass

Seeded FEL schemes can be used for generation of fully coherent radiation, which usually require a relatively uniform electron beam with constant current and energy. For a linear accelerator, the beam energy profile usually has an energy curvature due to the radio frequency curvature and wakefield effects. The energy chirped electron beam may be helpful in overcoming the sensitivity of the output power to the electron beam energy jitter. However, these energy chirps possibly degrade the FEL performances like the wavelength shifting and spectral bandwidth broadening [55,56]. In this section, simulation studies of the energy chirp effects on the HOK HGHG scheme for a single pass are presented.

The beam energy offset $\delta = \frac{E-E_0}{E_0}$ at the linac end can be described mathematically by a Taylor expansion:

$$\delta = \delta_0 + hs_i + h's_i^2 + \mathcal{O}(s^3), \tag{8}$$

where $\delta_0$ is the uncorrelated energy offset, $s_i$ is the particle longitudinal coordinate relative to the bunch center, $h = \frac{dE}{ds}\frac{1}{E}$ is a linear energy chirp with dimensions of $m^{-1}$, and $h' = \frac{d^2E}{ds^2}\frac{1}{E}$ is the quadratic chirp with dimensions of $m^{-2}$. The simulations are performed using the electron beam parameters summarized in Table I. The effect of a linear beam energy chirp on the final FEL central wavelength shifting for the HOK HGHG scheme is shown in Fig. 12(a). Similar to a standard single-stage HGHG scheme, the FEL central wavelength shifts in the HOK HGHG scheme when there is a linear beam energy chirp in the electron beam. In a realistic case, there are still nonlinear energy chirps in the electron beam. In the simulation, we use an electron beam with a quadratic energy chirp ($h' = 500\,000\ \mathrm{m}^{-2}$) exhibited in Fig. 12(b), as an example to study the nonlinear energy chirp effects on the HOK HGHG scheme. The other information of the electron beam is summarized in Table I. The effect of nonlinear energy chirp on the FEL bandwidth increase of the HOK HGHG scheme is shown in Fig. 12(c). It is found that the spectra bandwidth with a quadratic energy chirp ($h' = 500\,000\ \mathrm{m}^{-2}$) increases by a factor of 2 compared with the case without energy chirp.

### B. Resonator considerations

As already discussed in Ref. [39], a crucial factor is an appropriate choice of mirrors, since they determine the reflectivity and the power density limitations. For FLASH, with 5000 pulses per second, earlier simulations show that the estimated reflectivity of the mirrors and the absorbed power density is not a limiting factor. For cw FELs with a repetition rate of 1 MHz, this becomes more challenging. In Fig. 13, the reflectivity at 30 eV for a molybdenum mirror is shown as a function of the incoming angle of the radiation [57]. As can be seen, the reflectivity at 45° is about 40% and at 30° around 65%. Simulations show that, for stable operation of the resonator, the pulse energy is around 0.7 $\mu$J, which at 15-m distance means that the power density is 400 $\mathrm{mW/mm^2}$ for a cw machine running

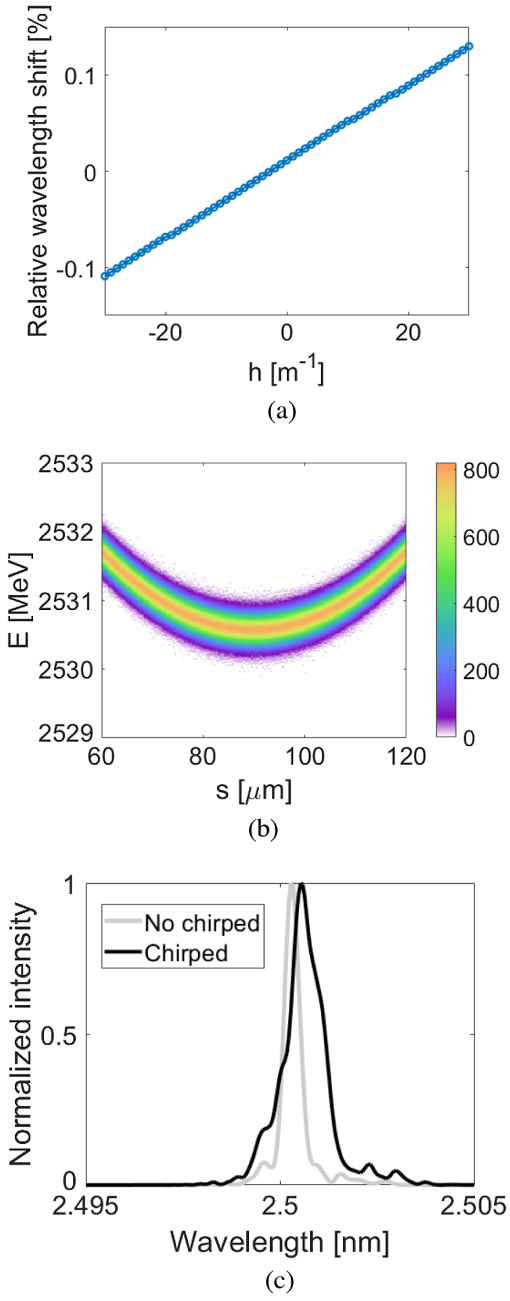


FIG. 12. (a) Impact of a linear energy chirp on the central wavelength relative shift of the final FEL radiation for the HOK HGHG scheme. (b) The longitudinal phase space of the electron beam with a quadratic energy chirp ($h' = 500\,000$ m$^{-2}$). (c) The output spectrum profiles for the HOK HGHG scheme at the end of the radiator (the black line represents the case with a quadratic energy chirp, and the gray line represents the case with no energy chirp).

at 1 MHz (for FLASH, this is only 2 mW/mm$^2$). Even under an angle of 30°, with the surface area increased by a factor of 2 and only a third of the power absorbed, the power density absorbed is still 70 mW/mm$^2$. Although this power density is possible if the mirror has active cooling, it is unlikely that this is a possibility considering the limited

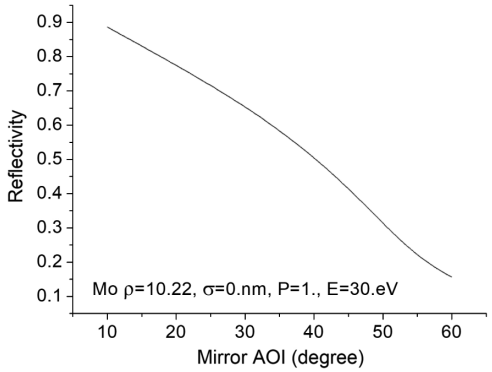


FIG. 13. Reflectivity of a molybdenum mirror for 30 eV photon energy for angles between 10° and 60°.

amount of space. Unfortunately, there is little information available at 24 eV (50 nm), where the simulations are performed. Because the reflectivity increases with decreasing photon energy, it is quite possible that at 24 eV the reflectivity is high enough. In order to verify this, an experimental program is in preparation to characterize several mirror materials in the photon energy range between 10 and 24 eV. In the meantime, other alternatives are being studied.

## VI. CONCLUSION AND OUTLOOK

Two harmonic optical klystron resonator configurations, namely, starting with an external seed laser and starting from shot noise, are proposed for seeding in high repetition rate free electron lasers. With the harmonic optical klystron as the seeding source, the efficiency of harmonic radiation generation at a comparatively high harmonic can be significantly enhanced when compared with a standard single-stage HGHG. In addition, there is no need of a large energy modulation in the in-cavity modulator to achieve a bunching at a quite high harmonic compared to the resonator-amplifier scheme in standard single-stage HGHG mode. Therefore, the intensity of the amplified light field in the first modulator is reduced to relieve the thermal load of the mirrors of the cavity. The single-pass and multipass simulation results prove that highly coherent, stable, short-wavelength radiation could be generated by the proposed schemes. Starting with a seed laser or from shot noise can have their own advantages and disadvantages, and the choice between the two options depends on the exact goals of a facility. Starting with a seed laser ensures synchronization with the laser and an almost immediate transition to a steady state. However, when starting from shot noise, it is possible to freely tune the resonator to shorter wavelengths and achieve wavelength tunability that depends only on the mirrors of the cavity and not on an external seed laser source. The latter option requires a cavity design that can adjust the gain to transition from buildup to steady state.

In comparison to other proposed schemes, our first stage of the harmonic optical klystron scheme with the optical cavity is used to obtain an energy modulation of the electron beam, instead of FEL amplification until saturation for direct use of the outcoupled radiation or harmonic cascade seeding [34,35]. On the other hand, the simulated schemes present similarities to the regular optical klystron scheme used for seeding [24,25] and the oscillator schemes [39]: In this case, the cavity is also used at a low power and with the sole goal of energy modulation of the electron beam. However, here we take one more step toward an easier and more flexible implementation of the seeded oscillator-amplifier scheme. The advantage of an optical klystron is that chicane 1 allows a tuning of the overall gain and can be used to regulate the energy modulation level despite possible power fluctuations in the cavity. Another important difference is that the power required in the first modulator is significantly lower in comparison to the power required in a standard HGHG scheme. A lower power or larger transverse size of the field can further relax the stability requirements. In addition, the mirrors can withstand higher repetition rates at this lower power, which is an important consideration for cw machines. Furthermore, the shorter wavelength radiation can be achieved by using the harmonic optical klystron configuration.

As an outlook, some practical considerations for the harmonic optical klystron resonator scheme need to be studied. For example, it is a necessity to look for experimental possibilities for the demonstration of the several challenges of this scheme, such as identifying suitable mirrors, measuring their response to high repetition rate radiation, and measuring the tolerances of the cavity. In addition, we study the energy chirp effects on this scheme for a single pass in this paper, and then we study the energy chirp effects on the multipass simulation results. As a next step, an EEHG scheme to achieve shorter wavelengths is planned. Start to end simulations, with a more realistic electron beam, are foreseen after a more detailed consideration of the resonator geometry and its limitations are studied.

## ACKNOWLEDGMENTS

The authors express their gratitude to Fabian Pannek and Weijie Fan for fruitful discussions in FEL physics and simulations. This work was supported by the National Natural Science Foundation of China (12122514 and 11975300) and Shanghai Science and Technology Committee Rising-Star Program (20QA1410100). G. P. was supported by the Impuls- und Vernetzungsfond der Helmholtz-Gemeinschaft e.V. within the CAS-Helmholtz International Laboratory on Free-Electron Laser Science and Technology (CHILFEL), Grant No. InterLabs-0002. B. F. was Funded by Chinese Academy of Sciences President's International Fellowship Initiative (PIFI), Grant No. 2020FSM0003.

[1] Z. Huang and K.-J. Kim, Review of x-ray free-electron laser theory, Phys. Rev. Accel. Beams **10**, 034801 (2007).
[2] C. Pellegrini, A. Marinelli, and S. Reiche, The physics of x-ray free-electron lasers, Rev. Mod. Phys. **88**, 015006 (2016).
[3] N. Huang, H. Deng, B. Liu, D. Wang, and Z. Zhao, Features and futures of x-ray free-electron lasers, Innovation **2**, 100097 (2021).
[4] A. Kondratenko and E. Saldin, Generation of coherent radiation by a relativistic electron beam in an ondulator, Part. Accel. **10**, 207 (1980), http://cds.cern.ch/record/6261107977/files/p207.pdf.
[5] R. Bonifacio, C. Pellegrini, and L. M. Narducci, Collective instabilities and high-gain regime in a free electron laser, Opt. Commun. **50**, 373 (1984).
[6] Z. Huang and K.-J. Kim, Three-dimensional analysis of harmonic generation in high-gain free-electron lasers, Phys. Rev. E **62**, 7295 (2000).
[7] G. Geloni, V. Kocharyan, and E. Saldin, A novel self-seeding scheme for hard x-ray FELs, J. Mod. Opt. **58**, 1391 (2011).
[8] J. Amman *et al.*, Demonstration of self-seeding in a hard-x-ray free-electron laser, Nat. Photonics **6**, 693 (2012).
[9] L. H. Yu, Generation of intense UV radiation by subharmonically seeded single-pass free-electron lasers, Phys. Rev. A **44**, 5178 (1991).
[10] L. H. Yu, M. Babzien, I. Ben-Zvi, L. Dimauro, A. Doyuran, W. Graves, E. Johnson, S. Krinsky, R.Malone, I. Pogorelsky, J. Skaritka, G. Rakowsky, L. Solomon, X. J. Wang, M. Woodle, V. Yakimenko, S. Biedron, J. N. Galayda, E. Gluskin, and I. Vasserman, High-gain harmonic-generation free-electron laser, Science **289**, 932 (2000).
[11] L. H. Yu and J. Wu, Theory of high gain harmonic generation: An analytical estimate, Nucl. Instrum. Methods Phys. Res., Sect. A **483**, 493 (2002).
[12] B. Liu *et al.*, Demonstration of a widely-tunable and fully-coherent high-gain harmonic-generation free-electron laser, Phys. Rev. Accel. Beams **16**, 020704 (2013).
[13] E. Allaria, P. Cinquegrana, S. Cleva, D. Cocco, M. Cornacchia, P. Craievich, I. Cudin, G. D'Auria, M. DalForno, M. Danailov, R. D. Monte, G. D. Ninno, P. Delgiusto, A. Demidovich, S. D. Mitri, B. Diviacco, A. Fabris, R. Fabris, W. Fawley, and M. Zangrando, Highly coherent and stable pulses from the Fermi seeded free-electron laser in the extreme ultraviolet, Nat. Photonics **6**, 699 (2012).
[14] G. Stupakov, Using the Beam-Echo Effect for Generation of Short-Wavelength Radiation, Phys. Rev. Lett. **102**, 074801 (2009).
[15] D. Xiang and G. Stupakov, Echo-enabled harmonic generation free electron laser, Phys. Rev. Accel. Beams **12**, 030702 (2009).
[16] D. Xiang, E. Colby, M. Dunning, S. Gilevich, C. Hast, K. Jobe, D. McCormick, J. Nelson, T. O. Raubenheimer, K. Soong, G. Stupakov, Z. Szalata, D. Walz, S. Weathersby, M. Woodley, and P.-L. Pernet, Demonstration of the Echo-Enabled Harmonic Generation Technique for Short-Wavelength Seeded Free Electron Lasers, Phys. Rev. Lett. **105**, 114801 (2010).
[17] D. Xiang, E. Colby, M. Dunning, S. Gilevich, C. Hast, K. Jobe, D. McCormick, J. Nelson, T. O. Raubenheimer,

K. Soong, G. Stupakov, Z. Szalata, D. Walz, S. Weathersby, and M. Woodley, Evidence of High Harmonics from Echo-Enabled Harmonic Generation for Seeding X-Ray Free Electron Lasers, Phys. Rev. Lett. **108**, 024802 (2012).

[18] Z. T. Zhao *et al.*, First lasing of an echo-enabled harmonic generation free-electron laser, Nat. Photonics **6**, 360 (2012).

[19] E. Hemsing, M. Dunning, B. Garcia, C. Hast, T. Raubenheimer, G. Stupakov, and D. Xiang, Echo-enabled harmonics up to the 75th order from precisely tailored electron beams, Nat. Photonics **10**, 512 (2016).

[20] C. Feng *et al.*, Coherent extreme ultraviolet free-electron laser with echo-enabled harmonic generation, Phys. Rev. Accel. Beams **22**, 050703 (2019).

[21] P. Ribič, A. Abrami, L. Badano, M. Bossi, H.-H. Braun, N. Bruchon, F. Capotondi, D. Castronovo, M. Cautero, P. Cinquegrana, M. Coreno, M. Couprie, I. Cudin, M. Danailov, G. D. Ninno, A. Demidovich, S. D. Mitri, B. Diviacco, W. Fawley, and E. Allaria, Coherent soft x-ray pulses from an echo-enabled harmonic generation free-electron laser, Nat. Photonics **13**, 555 (2019).

[22] C. Feng and Z. Zhao, A storage ring based free-electron laser for generating ultrashort coherent EUV and x-ray radiation, Sci. Rep. **7**, 4724 (2017).

[23] X. Wang, C. Feng, T. Liu, Z. Zhang, C.-Y. Tsai, J. Wu, C. Yang, and Z. Zhao, Angular dispersion enhanced prebunch for seeding ultrashort and coherent EUV and soft x-ray free-electron laser in storage rings, J. Synchrotron Radiat. **26**, 677 (2019).

[24] J. Yan *et al.*, Self-Amplification of Coherent Energy Modulation in Seeded Free-Electron Lasers, Phys. Rev. Lett. **126**, 084801 (2021).

[25] G. Paraskaki, E. Allaria, E. Schneidmiller, and W. Hillert, High repetition rate seeded free electron laser with an optical klystron in high-gain harmonic generation, Phys. Rev. Accel. Beams **24**, 120701 (2021).

[26] X. Wang, C. Feng, B. Faatz, W. Zhang, and Z. Zhao, High-repetition-rate seeded free-electron laser with direct-amplification of an external coherent laser, New J. Phys. **24**, 033013 (2022).

[27] Z. Zhao, D. Wang, Q. Gu, L. Yin, G. Fang, M. Gu, Y. Leng, Q. Zhou, B. Liu, C. Tang, W. Huang, Z. Liu, and H. Jiang, SXFEL: A soft x-ray free electron laser in China, Synchrotron Radiat. News **30**, 29 (2017).

[28] K.-J. Kim and Y. V. Shvyd'ko, Tunable optical cavity for an x-ray free-electron-laser oscillator, Phys. Rev. Accel. Beams **12**, 030703 (2009).

[29] K. Li and H. Deng, Systematic design and three-dimensional simulation of x-ray FEL oscillator for Shanghai Coherent Light Facility, Nucl. Instrum. Methods Phys. Res., Sect. A **895**, 40 (2018).

[30] M. Opromolla, A. Bacci, M. Rossetti Conti, A. R. Rossi, G. Rossi, L. Serafini, A. Tagliaferri, and V. Petrillo, High repetition rate and coherent free-electron laser oscillator in the tender x-ray range tailored for linear spectroscopy, Appl. Sci. **11**, 5892 (2021).

[31] Z. Huang and R. D. Ruth, Fully Coherent X-Ray Pulses from a Regenerative-Amplifier Free-Electron Laser, Phys. Rev. Lett. **96**, 144801 (2006).

[32] B. W. J. McNeil, N. R. Thomson, D. J. Dunning, J. G. Karssenber, P. J. M. V. der Slot, and K.-J. Boller, A design for the generation of temporally-coherent radiation pulses in the VUV and beyond by a self-seeding high-gain free electron laser amplifier, New J. Phys. **9**, 239 (2007).

[33] P. J. M. van der Slot and H. P. Freund, Three-dimensional, time-dependent analysis of high- and low-Q free-electron laser oscillators, Appl. Sci. **11**, 4978 (2021).

[34] K. Li, J. Yan, C. Feng, M. Zhang, and H. Deng, High brightness fully coherent x-ray amplifier seeded by a free-electron laser oscillator, Phys. Rev. Accel. Beams **21**, 040702 (2018).

[35] V. Petrillo, A. Bacci, A. R. Rossi, L. Serafini, I. Drebot, M. R. Conti, M. Ruijter, M. Opromolla, S. Samsam, F. Broggi, G. Ghiringhelli, E. Puppin, G. Rossi, and A. tagliaferri, Coherent, high repetition rate tender x-ray free-electron laser seeded by an extreme ultra-violet free-electron laser oscillator, New J. Phys. **22**, 073058 (2020).

[36] N. S. Mirian, M. Opromolla, G. Rossi, L. Serafini, and V. Petrillo, High-repetition rate and coherent free-electron laser in the tender x rays based on the echo-enabled harmonic generation of an ultraviolet oscillator pulse, Phys. Rev. Accel. Beams **24**, 050702 (2021).

[37] S. Ackermann, B. Faatz, V. Grattoni, M. M. Kazemi, T. Lang, C. Lechner, G. Paraskaki, J. Zemella, G. Geloni, S. Serkez, T. Tanikawa, and W. Hillert, Novel method for the generation of stable radiation from free-electron lasers at high repetition rates, Phys. Rev. Accel. Beams **23**, 071302 (2020).

[38] G. Paraskaki, V. Grattoni, T. Lang, J. Zemella, B. Faatz, and W. Hillert, Optimization and stability of a high-gain harmonic generation seeded oscillator amplifier, Phys. Rev. Accel. Beams **24**, 034801 (2021).

[39] G. Paraskaki, S. Ackermann, B. Faatz, G. Geloni, T. Lang, F. Pannek, L. Schaper, and J. Zemella, Advanced scheme to generate MHz, fully coherent FEL pulses at nm wavelength, Appl. Sci. **11**, 6058 (2021).

[40] Z. Zhu, Z. T. Zhao, D. Wang, Z. H. Yang, and L. Yin, SCLF: An 8-GeV CW SCRF linac-based x-ray FEL facility in Shanghai, in *Proceedings of the 38th International Free Electron Laser Conference (FEL'17)* (JACoW, Geneva, 2017), pp. 182–184, https://accelconf.web.cern.ch/fel2017/papers/mop055.pdf.

[41] A. Brachmann, M. Dunham, and J. Schmerge, LCLS-II—Status and upgrades, in *Proceedings of the 39th International Free Electron Laser Conference (FEL'19)* (JACoW, Geneva, 2019), pp. 772–775, http://jacow.org/fel2019/papers/fra02.pdf.

[42] J. Rossbach, J. R. Schneider, and W. Wurth, 10 years of pioneering x-ray science at the free-electron laser flash at DESY, Phys. Rep. **808**, 1 (2019).

[43] W. Ackermann *et al.*, Operation of a free-electron laser from the extreme ultraviolet to the water window, Nat. Photonics **1**, 336 (2007).

[44] H. Weise and W. Decking, Commissioning and first lasing of the european XFEL, in *Proceedings of the 38th International Free Electron Laser Conference (FEL'17)* (JACoW, Geneva, 2017), pp. 9–13, https://accelconf.web.cern.ch/fel2017/papers/moc03.pdf.

[45] G. Penco, Optical klystron enhancement to self amplified spontaneous emission at FERMI, Photonics **4**, 15 (2017).

[46] D. J. Dunning, N. R. Thompson, and B. W. J. McNeil, Design study of an HHG-seeded harmonic cascade free-electron laser, J. Mod. Opt. **58**, 1362 (2011).

[47] S. Reiche, Genesis 1.3: A fully 3D time-dependent FEL simulation code, Nucl. Instrum. Methods Phys. Res., Sect. A **429**, 243 (1999).

[48] I. Agapov, G. Geloni, S. Tomin, and I. Zagorodnov, Ocelot: A software framework for synchrotron light source and FEL studies, Nucl. Instrum. Methods Phys. Res., Sect. A **768**, 151 (2014).

[49] E. Hemsing, G. Stupakov, D. Xiang, and A. Zholents, Beam by design: Laser manipulation of electrons in modern accelerators, Rev. Mod. Phys. **86**, 897 (2014).

[50] J. Qika, Analysis of modulation parameters for high repetition rate seeded FEL, Nucl. Instrum. Methods Phys. Res., Sect. A **1015**, 165767 (2021).

[51] G. Penco, G. Perosa, E. Allaria, S. Di Mitri, E. Ferrari, L. Giannessi, S. Spampinati, C. Spezzani, and M. Veronese, Enhanced seeded free electron laser performance with a "cold" electron beam, Phys. Rev. Accel. Beams **23**, 120704 (2020).

[52] S. Reiche, Overview of seeding methods for FELS, in *Proceedings of the 4th International Particle Accelerator Conference, IPAC-2013, Shanghai, China, 2013* (JACoW, Geneva, 2013), pp. 2063–2067.

[53] E. Takahashi, Y. Nabekawa, and K. Midorikawa, Generation of 10-$\mu j$ coherent extreme-ultraviolet light by use of high-order harmonics, Opt. Lett. **27**, 1920 (2002).

[54] Z.-Y. Zhao, H.-T. Li, and Q.-K. Jia, Effect of cavity length detuning on the output characteristics for the middle infrared FEL oscillator of FELiChEM, Chin. Phys. C **41**, 108101 (2017).

[55] C. Feng, D. Wang, and Z. T. Zhao, Study of the energy chirp effects on seeded FEL schemes at SDUV-FEL, in *Proceedings of the 3rd International Particle Accelerator Conference (IPAC'12)* (JACoW, Geneva, 2012), pp. 1724–1726, https://accelconf.web.cern.ch/IPAC2012/papers/tuppp056.pdf.

[56] G. Paraskaki, S. Ackermann, B. Faatz, V. Grattoni, C. Lechner, M. Mehrjoo, G. Geloni, S. Serkez, T. Tanikawa, and W. Hillert, Study of a seeded oscillator-amplifier, in *Proceedings of the 39th International Free Electron Laser Conference (FEL'19)* (JACoW, Geneva, 2019), pp. 238–241, https://accelconf.web.cern.ch/fel2019/papers/tup077.pdf.

[57] B. Henke, E. Gullikson, and J. Davis, X-ray interactions: Photoabsorption, scattering, transmission, and reflection at $E = 50 - 30,000$ eV, $Z = 1 - 92$, At. Data Nucl. Data Tables **54**, 181 (1993).